arXiv:1607.07424v4 [cond-mat.mes-hall] 15 Nov 2016

Goos-Hänchen shift of a spin-wave beam transmitted through anisotropic interface between two ferromagnets

P. Gruszecki,[1] M. Mailyan,[2] O. Gorobets,[2,3] and M. Krawczyk[1]
[1] *Faculty of Physics, Adam Mickiewicz University in Poznan, Umultowska 85, Poznań, 61-614, Poland*
[2] *National Technical University of Ukraine "Kyiv Polytechnic Institute", 37 Peremogy ave., 03056, Kyiv, Ukraine*
[3] *Institute of Magnetism, National Academy of Sciences of Ukraine, 36-b Vernadskogo st., 03142, Kyiv, Ukraine*
(Dated: November 16, 2016)

The main object of investigation in magnonics, spin waves (SWs) are promising information carriers. Presently the most commonly studied are plane wave-like SWs and SWs propagating in confined structures, such as waveguides. Here we consider a Gaussian SW beam obliquely incident on an ultra-narrow interface between two identical ferromagnetic materials. We use an analytical model and micromagnetic simulations for an in-depth analysis of the influence of the interface properties, in particular the magnetic anisotropy, on the transmission of the SW beam. We derive analytical formulas for the reflectance, transmittance, phase shift and Goos-Hänchen (GH) shift for beams reflected and refracted by an interface between two semi-infinite ferromagnetic media; the results for the refracted beam are the first to be reported to date. The GH shifts in SW beam reflection and transmission are confirmed by micromagnetic simulations in the thin-film geometry. We demonstrate the dependence of the characteristic properties on the magnetic anisotropy at the interface, the angle of incidence and the frequency of the SWs. We also propose a method for the excitation of high-quality SW beams in micromagnetic simulations.

I. INTRODUCTION

Moore's law in its basic form postulated in 1965 [1], stating that the number of transistors in a dense integrated circuit (or chip's doubles approximately every two years, is now nearing its end [2]. In the light of the still increasing demand for computational resources, the presently dominating CMOS circuits are reaching their limits in terms of miniaturization, performance and energy consumption [2, 3]. Moreover, the costs are rising while the benefits of further miniaturization are decreasing [2]. This brings about the necessity to create a new class of devices with enhanced performance and functionality for various applications to supplement or even replace CMOS circuits [4, 5]. Spin waves (SWs) are among the potential candidates for replacement of electric charges as information carriers [6–8].

The main object of investigation in the emerging branch of modern magnetism known as magnonics [9, 10], SWs are magnetization excitations propagating without charge transport. This excludes Joule heating and implies that the application of SWs in computing devices could significantly reduce the energy consumption with respect to the charge-based alternatives [5, 11]. Spin waves have frequencies ranging from several GHz to hundreds of GHz with wavelengths 4 to 5 orders of magnitude shorter than those of electromagnetic waves of the same frequencies. Moreover, even in homogeneous planar structures SWs have a nontrivial dispersion relation, resulting in an exceptional richness of potential properties that could be used for SW manipulation; these properties have no counterpart in photonics and electronics [6].

Potentially, SWs guarantee high operating frequencies and low energy consumption with preserved CMOS level of miniaturization and possible integration with present CMOS circuits. Solutions known from photonics, spintronics and electronics can be applied in magnonics as well. Furthermore, the use of SWs as information carriers would pave the way to wave-based non-Boolean computing [13], holographic memory [12, 14] or the physical realization of neural networks [15]. Crucial in these approaches is the manipulation of both amplitude and phase of the SWs. In magnonics this can be realized by means of magnonic crystals or SW scattering by disturbances such as holes [14], domain walls [16] or magnetic elements placed on waveguide cross junctions [12]. Another possible approach, which has emerged in modern photonics for electromagnetic waves, is based on the use of materials referred to as metasurfaces for wave manipulation at sub-wavelength distances [17].

The reflection and refraction of SWs are determined by the magnetic properties of the ferromagnetic media and by the interface boundary conditions. In the theoretical and experimental studies of spin-wave reflection [18, 19] and refraction [19–21] reported to date SWs are mostly treated as plane waves. Other kinds of excitations, specifically, coherent low-divergence spin-wave beams (SWBs), the application of which would open new possibilities, have not been explored to date. There are only a few theoretical and experimental studies on the formation of low-frequency SW beams; research in this field is hampered by caustics, nonlinear effects and difficulties related to excitation by nanooscillators or width-modulated microwave transducers [22–30].

From the theoretical point of view the study of SW reflection and refraction can be regarded as the investigation of the amplitude and phase changes (in relation to the incident SWs) that the reflected and transmitted SWs, respectively, undergo at the interface. Very convenient parameters in that study are reflectance R (the power ratio of the reflected and incident SWs) and transmittance T (the power ratio of the transmitted and

incident SWs), and the phase shifts $\Delta\varphi_{\rm r}$ and $\Delta\varphi_{\rm t}$ of the reflected and transmitted waves, respectively, in relation to the incident SWs. It is noteworthy that one of the physical consequences of those phase shifts can be the occurrence of a lateral shift $\Delta_{\rm r}$ or $\Delta_{\rm t}$ of the beam spots along the interface in the respective effects. Known from optics and first demonstrated for reflected light in 1947 by H. Hänchen and F. Goos [31], this wave phenomenon is referred to as the Goos-Hänchen effect (GHE). It occurs also in acoustics, where it is known as the Schoch displacement [32], in electronics [33] and in neutron waves [34].

Although shown theoretically not to occur in magnetostatic waves (i.e., SWs in the limit of negligible exchange interaction [35]), the GHE has been demonstrated, also theoretically, in reflection of purely exchange SWs (i.e., high-frequency SWs with neglected dipole-dipole interactions) by an interface between two semi-infinite ferromagnetic films [36]. The effect was later confirmed by micromagnetic simulations for exchange-dipolar SWs reflected by the edge of a magnetic thin film [45]. The magnetic properties at the film edge have been shown to be crucial for the lateral shift of the SW beam; specifically, the value of $\Delta_{\rm r}$ is very sensitive even to slight changes in the magnetic surface anisotropy at the film edge [48].

Full elucidation of SW reflection and refraction and the influence of the boundary conditions on the reflectance, transmittance and phase shifts would open the possibility of manipulating not only the amplitudes, but also the phases of SWs at very short distances. This could be critical for the future development of magnonic devices.

In this paper we analyze theoretically and numerically SW refraction by an ultra-narrow interface between two ferromagnetic materials. We consider high-frequency SWs and study the influence of the interface on their reflection and, especially, refraction. In particular, we investigate the role of the magnetic anisotropy introduced at the interface and focus on the transmittance and the GH shifts of the transmitted SW beams. We propose an analytical model for purely exchange SWs in two semi-infinite materials, and derive formulas for the reflectance and transmittance and the respective GH shifts.

These results are verified by micromagnetic simulations (MSs) of a SW beam passing through an interface between two semi-infinite ferromagnetic thin films. The performed MSs take also account of the dipolar interaction. The data obtained demonstrate that the reflection and transmission of SWs are sensitive to even slight changes in the magnetic anisotropy introduced at the interface, the thickness of which is much smaller than the wavelength of the SWs. The transmittance is shown to decrease and the GH shift to grow with decreasing SW frequency and angle of incidence.

Our findings can be of interest and use wherever SW phase and amplitude manipulation is required, including logic and microwave applications. Moreover, we believe that the control of SWs at sub-wavelength distances can initiate a new research direction, which, by analogy with photonics, can be called magnonic metasurfaces. We have also developed an efficient method for SWB excitation in MSs, which can be easily exploited in magnonic studies.

The paper is organized as follows. In Sec. II we present the analytical model of SW reflection and refraction, and the micromagnetic simulations. The obtained analytical results and simulation data are discussed in Sec. III. Conclusions are provided in Sec. IV. The derived analytical formulas for the GH shifts are presented in Appendix A, while Appendix B describes the method of SWB excitation used in the MSs.

II. METHODS

A. Analytical model

Let us begin by constructing an analytical model of SW reflection and refraction by an interface, extending along the y- and z-axes, between two semi-infinite ferromagnetic materials FM-1 and FM-2 (Fig. 1). We assume uniform magnetization of the system by an external magnetic field $\mathbf{H} = [0, 0, H_0]$ parallel to the interface (yOz plane) and perpendicular to the plane of incidence (xOy plane). In both materials we consider the same direction of magnetocrystalline anisotropy, parallel to that of the surface magnetic anisotropy, along the z-axis: $\mathbf{n}^{(1)} = \mathbf{n}^{(2)} = \mathbf{e}_z$. We will only analyze here high-frequency short-wavelength SWs (i.e., exchange SWs), in which case the influence of the dipolar interaction can be neglected. The considered SWs are also assumed to be uniform along the z-axis.

The total energy of the system composed of two ferromagnetic materials (indicated with superscripts $^{(1)}$ and $^{(2)}$) can be written as:

$$W = \int\limits_V dv \Big[w_{\rm H}^{(1)} + w_{\rm H}^{(2)} + w_{\rm ex}^{(1)} + w_{\rm ex}^{(2)} + w_{\rm anis}^{(1)} + w_{\rm anis}^{(2)} + w_{\rm ex}^{(12)} + w_{\rm anis}^{(12)} \Big], \tag{1}$$

where the integration runs over the whole volume.

The term $w_{\rm H}^{(l)} = -\mathbf{M}^{(l)} \cdot \mathbf{H}$ is the Zeeman energy density, where $\mathbf{M}^{(l)} = \Big[m_x^{(l)}, m_{y,}^{(l)} M_l \Big]$ denotes the magnetization vector in the l-th ferromagnet and M_l is its saturation magnetization.

The next two terms, $w_{\rm ex}^{(l)} = \dfrac{1}{2}\alpha_l(x) \left(\nabla \mathbf{M}^{(l)}\right)^2$, are the exchange energy densities; $\alpha_l = A_l/M_l^2$ denotes the exchange length and A_l is the exchange constant. The term $w_{\rm anis}^{(l)} = -\dfrac{1}{2}\beta_l(x) \left(\mathbf{M}^{(l)} \cdot \mathbf{n}^{(l)}\right)^2$ is the magnetic anisotropy energy density in the l-th ferromagnet; $\beta_l = K_l/M_l^2$, where K_l is the uniaxial magnetic anisotropy constant, and $\mathbf{n}^{(l)}$ is a unit vector pointing in the direction of the easy axis in the l-th ferromagnet.

The term $w_{\rm ex}^{(12)} = A_{12}\mathbf{M}^{(1)} \cdot \mathbf{M}^{(2)} \Theta_{\rm H}(x) \Theta_{\rm H}(-x + \delta)$ is the energy density of interlayer exchange coupling at the

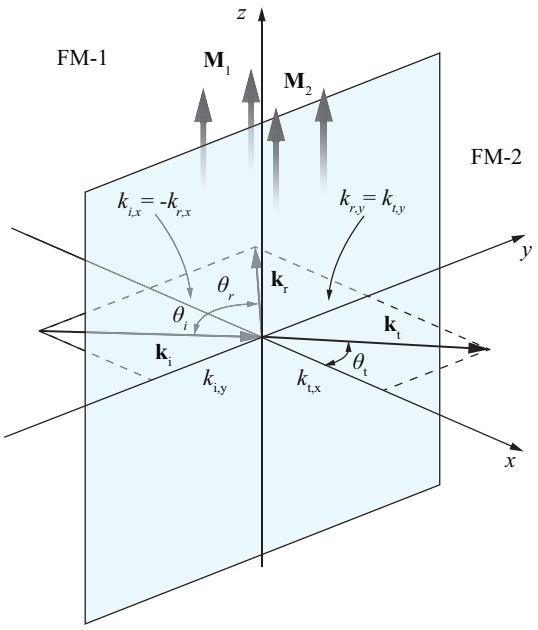

Figure 1. Schematic representation of the system used in the analytical model. Two semi-infinite ferromagnetic materials, FM1 and FM2, are separated by an interface (gray plane) lying in the yOz plane. The external magnetic field, static magnetization and anisotropy field are all oriented along the z-axis. The plane of incidence is the xOy plane.

interface between the ferromagnets; $\Theta_{\rm H}(x)$ is the Heaviside step function, δ the width of the interface, and A_{12} a parameter of uniform exchange interaction; $A_{12} = \xi A_{\rm int,S}/M_{\rm int}^2$, where $A_{\rm int,S}$ denotes the effective surface exchange constant of the interface ($A_{\rm int,S} = A_{\rm int}/\delta$, with $A_{\rm int}$ being the exchange constant of the interface region), $M_{\rm int}$ is the saturation magnetization of the interface, and ξ a proportionality coefficient (we assume $\xi = 400$).

The last term in Eq. (1), $w_{\rm anis}^{(12)} = -\frac{1}{2}\left[\beta_{12}\left(\mathbf{M}^{(1)}\cdot\mathbf{n}^{(1)}\right)\left(\mathbf{M}^{(2)}\cdot\mathbf{n}^{(2)}\right)\right]\Theta_{\rm H}(x)\Theta_{\rm H}(-x+\delta)$, is the energy density of surface magnetic anisotropy at the interface; $\beta_{12} = K_{12}/M_{\rm int}^2$ is an anisotropy parameter, with K_{12} denoting the uniaxial magnetic anisotropy constant at the interface (which can be regarded as stemming from the surface magnetic anisotropy, $K_{12} \equiv K_{\rm S}/\delta$).

The SW dynamics in this system can be described by the Landau-Lifshitz (LL) equations for both ferromagnetic materials:

$$\begin{cases} \dfrac{\partial \mathbf{M}^{(1)}}{\partial t} = & |\gamma|\,\mathbf{M}^{(1)}\times\mathbf{H}_{\rm eff}^{(1)} \\ \dfrac{\partial \mathbf{M}^{(2)}}{\partial t} = & |\gamma|\,\mathbf{M}^{(2)}\times\mathbf{H}_{\rm eff}^{(2)}, \end{cases} \tag{2}$$

where γ is the gyromagnetic ratio. We will use the linear approximation, based on the assumption that the dynamic components of the magnetization are much smaller than the saturation magnetization, $m_{x,y}^{(l)} \ll M_l$, and the latter can be treated as constant. The effective magnetic field $\mathbf{H}_{\rm eff}^{(l)}$ in each material can be determined as the functional derivative of the total energy, defined in Eq. (1), with respect to the magnetization vector:

$$\mathbf{H}_{\rm eff}^{(l)} = -\frac{\delta W}{\delta \mathbf{M}^{(l)}} = -\frac{\partial w}{\partial \mathbf{M}^{(l)}} + \sum_{\zeta\in\{x,y,z\}} \frac{\mathrm{d}}{\mathrm{d}\zeta}\frac{\partial w}{\partial\left(\dfrac{\mathrm{d}\mathbf{M}}{\mathrm{d}\zeta}\right)}, \tag{3}$$

where w is the energy density, the integral kernel in Eq. (1).

Assuming plane-wave solutions of the LL equations (2), $m_{x,y}^{(l)} \propto \exp[i(\mathbf{k}_l\cdot\mathbf{r} - \omega_l t)]$, in each of the ferromagnetic materials, we obtain the SW dispersion relation:

$$\omega_l(\mathbf{k}_l) = |\gamma|\left(H_0 + \beta_l M_l + M_l\alpha_l k_l^2\right), \tag{4}$$

where $\mathbf{k}_l$ is the wavevector and ω_l the angular frequency of SWs in the l-th ferromagnet [38].

The LL equations (2) can be integrated over the interface region in the limit of infinitely narrow interface [58]:

$$\int_{-0}^{+0}\left[\frac{\partial \mathbf{M}^{(l)}}{\partial t} - |\gamma|\,\mathbf{M}^{(l)}\times\mathbf{H}_{\rm eff}^{(l)}\right]dx = 0. \tag{5}$$

The integration of the above equations (for $l = 1$ and $l = 2$) with the effective magnetic field as expressed in (3) yields the boundary conditions in the form of a set of equations linking the dynamic components of the magnetization on both sides of the interface:

$$\begin{cases} \left(A_{12}m_n^{(2)} + Dm_n^{(1)} + \alpha_1\dfrac{\partial m_n^{(1)}}{\partial x}\right)\Big|_{x=-0} = 0 \\ \left(A_{12}m_n^{(1)} + Cm_n^{(2)} - \alpha_2\dfrac{\partial m_n^{(2)}}{\partial x}\right)\Big|_{x=+0} = 0, \end{cases} \tag{6}$$

where $n = x, y$, $D = -\left[(A_{12}-\beta_{12})\,\zeta - \beta_1\right]\delta$, $C = -\left[(A_{12}-\beta_{12})/\zeta + \beta_2\right]\delta$, and $\zeta = M_2/M_1$. The physical meaning of the parameters D and C is that of effective values obtained by averaging the finite width δ over the interface region (see Ref. [37], Section 4).

Having the boundary conditions (6), we can derive the Fresnel equations for exchange SWs. To this end we describe incident and reflected circularly polarized SWs in FM-1 and refracted SWs in FM-2 as monochromatic plane waves:

$$\begin{cases} \left(m_x^{(1)} + im_y^{(1)}\right) = & \mathrm{e}^{i(\mathbf{k}_{\rm i}\cdot\mathbf{r}-\omega t)} + r\mathrm{e}^{i(\mathbf{k}_{\rm r}\cdot\mathbf{r}-\omega t+\varphi_{\rm r})} \\ \left(m_x^{(2)} + im_y^{(2)}\right) = & t\mathrm{e}^{i(\mathbf{k}_{\rm t}\cdot\mathbf{r}-\omega t+\varphi_{\rm t})}, \end{cases} \tag{7}$$

where r and t are the reflection and transmission coefficients, respectively. A SW incident at an angle $\theta_{\rm i}$ has a wavevector $\mathbf{k}_{\rm i} = (k_{{\rm i},x}\mathbf{e}_x + k_{{\rm i},y}\mathbf{e}_y) = k_{\rm i}(\mathbf{e}_x\cos\theta_{\rm i} + \mathbf{e}_y\sin\theta_{\rm i})$. Similarly, the reflected and transmitted SWs have wavevectors $\mathbf{k}_{\rm r} = (k_{{\rm r},x}\mathbf{e}_x + k_{{\rm r},y}\mathbf{e}_y)$ and $\mathbf{k}_{\rm t} =$

$(k_{\mathrm{t},x}\mathbf{e}_x + k_{\mathrm{t},y}\mathbf{e}_y)$, respectively. Due to the translational symmetry along the interface the wavevector component tangential to the interface is conserved, $k_{\mathrm{i},y} = k_{\mathrm{r},y} = k_{\mathrm{t},y}$. Moreover, the isotropic dispersion relation implies $k_{\mathrm{i},x} = -k_{\mathrm{r},x}$.

The substitution of Eq. (7) into the boundary conditions (6) yields the Fresnel amplitude coefficients for reflected and refracted SWs:

$$r = \sqrt{\frac{\left(A_{12}^2 - CD - \alpha_1\alpha_2 k_{\mathrm{r},x}k_{\mathrm{t},x}\right)^2 + \left(D\alpha_2 k_{\mathrm{t},x} - C\alpha_1 k_{\mathrm{r},x}\right)^2}{\left(A_{12}^2 - CD + \alpha_1\alpha_2 k_{\mathrm{r},x}k_{\mathrm{t},x}\right)^2 + \left(D\alpha_2 k_{\mathrm{t},x} + C\alpha_1 k_{\mathrm{r},x}\right)^2}}, \tag{8}$$

$$t = \frac{2A_{12}\alpha_1 k_{\mathrm{r},x}}{\sqrt{\left(A_{12}^2 - CD + \alpha_1\alpha_2 k_{\mathrm{r},x}k_{\mathrm{t},x}\right)^2 + \left(D\alpha_2 k_{\mathrm{t},x} + C\alpha_1 k_{\mathrm{r},x}\right)^2}}. \tag{9}$$

Reflectance R and transmittance T describe how the energy carried by a SW changes as a result of reflection and refraction, respectively, in relation to the incident wave. Thus, in addition to their dependence on the amplitude coefficients, those parameters can also vary with angle of incidence. In the case of reflection $\theta_\mathrm{i} = \theta_\mathrm{r}$ and

$$R = r^2. \tag{10}$$

In refraction:

$$T = t^2\frac{\cos(\theta_\mathrm{t})}{\cos(\theta_\mathrm{i})}. \tag{11}$$

We can also determine the phase differences φ_t and φ_r between transmitted/reflected and incident SWs. The phase shift of a reflected SW with respect to the incident wave is:

$$\begin{aligned}\varphi_\mathrm{r} = &\operatorname{arcctg}\left(-\frac{D\alpha_2\sqrt{k_\mathrm{t}^2 - k_{\mathrm{r},y}^2} + C\alpha_1\sqrt{k_\mathrm{r}^2 - k_{\mathrm{r},y}^2}}{A_{12}^2 - CD + \alpha_1\alpha_2\sqrt{(k_\mathrm{r}^2 - k_{\mathrm{r},y}^2)}\sqrt{(k_\mathrm{t}^2 - k_{\mathrm{r},y}^2)}}\right)\\ &+ \operatorname{arcctg}\left(\frac{D\alpha_2\sqrt{k_\mathrm{t}^2 - k_{\mathrm{r},y}^2} - C\alpha_1\sqrt{k_\mathrm{r}^2 - k_{\mathrm{r},y}^2}}{A_{12}^2 - CD - \alpha_1\alpha_2\sqrt{(k_\mathrm{r}^2 - k_{\mathrm{r},y}^2)}\sqrt{(k_\mathrm{t}^2 - k_{\mathrm{r},y}^2)}}\right).\end{aligned} \tag{12}$$

The phase of a transmitted SW is shifted by:

$$\varphi_\mathrm{t} = \operatorname{arcctg}\left(-\frac{D\alpha_2\sqrt{k_\mathrm{t}^2 - k_{\mathrm{r},y}^2} + C\alpha_1\sqrt{k_\mathrm{r}^2 - k_{\mathrm{r},y}^2}}{A_{12}^2 - CD + \alpha_1\alpha_2\sqrt{(k_\mathrm{r}^2 - k_{\mathrm{r},y}^2)}\sqrt{(k_\mathrm{t}^2 - k_{\mathrm{r},y}^2)}}\right). \tag{13}$$

According to Refs. [36, 39], there is the following relation between the phase shifts in reflection and transmission and the respective GH shifts:

$$\Delta_{\mathrm{r(t)}} = -\frac{\partial\varphi_{\mathrm{r(t)}}}{\partial k_{\mathrm{r(t)},y}}, \tag{14}$$

where the tangential components of the reflected and transmitted wavevectors are equal, $k_{\mathrm{r},y} = k_{\mathrm{t},y}$. The final formulas for the GH shifts are presented in Appendix A.

Below we assume FM-1 and FM-2 to be the same material. Thus, in Eq. (11) $\theta_\mathrm{i} = \theta_\mathrm{t}$, which implies $T = t^2$.

B. Micromagnetic simulations

Micromagnetic simulations (MSs) are a proven and efficient tool for the calculation of the SW dynamics in various geometries [49–52]. We have used the GPU-accelerated MS program MuMax3 [44], which solves the time-dependent LL equation with a Landau damping term by the finite difference method.

Shown in Fig. 2, the simulated system consists of two extended Py thin films with dimensions $L_x/2 \times L_y \times L_z$, separated by a narrow interface slice with a width $\delta = 2$ nm. The interface is parallel to the yOz plane and has a magnetic anisotropy different from that in Py. The surface magnetic anisotropy K_S at the interface between the Py films is introduced in the MSs by assuming a uniaxial magnetic anisotropy value K_{12} in the interface slice. Its all other parameters are the same as elsewhere in this magnetic system, comprising the films and the interface region.

We assumed a Py saturation magnetization $M_1 = M_2 = M_\mathrm{S} = 0.7 \times 10^3$ Gs, and an exchange constant $A_1 = A_2 = 1.1 \times 10^{-6}$ erg/cm. The simulations were performed for a magnetically saturated film with a thick-

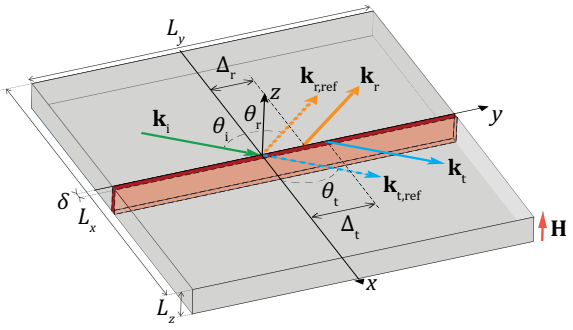

Figure 2. Schematic representation of the simulated system. The structure is a thin film with a thickness L_z much smaller than its lateral dimensions L_x and L_y. The red area at $y = 0$ is an interface layer with a width δ; $\mathbf{k}_\mathrm{i}$, $\mathbf{k}_\mathrm{r}$ and $\mathbf{k}_\mathrm{t}$ are the wavevectors of incident, reflected and transmitted SW beams, respectively; the wavevectors of GH shift-free reference reflected and refracted beams are denoted as $\mathbf{k}_\mathrm{r,ref}$ and $\mathbf{k}_\mathrm{t,ref}$, respectively; Δ_t is the total lateral shift (along the interface) of the transmitted SW beam with respect to the incident beam.

ness $L_z = 10$ nm. A magnetic field $H_0 = 15$ kOe was applied along the z-axis. The structure was discretized into cuboid elements with in-plane dimensions 2 nm × 2 nm, much smaller than both the exchange length of Py (6 nm) and the wavelength of the SWs. In the z direction each cuboid extended across the thickness of the film. To speed up the simulations, the lateral dimensions $L_x \times L_y$ of the simulated area were assumed depending on the angle of incidence. Nonetheless, in all the cases considered these dimensions were large enough (several μm) to prevent the influence of the finite size of the system on the propagation of SWs. Moreover, absorbing boundary conditions were assumed in order to prevent SW reflection by the edges of the simulated structure [45]

The MSs were performed in two stages, static and dynamic. In the first, static stage an equilibrium magnetic configuration of the system was obtained by relaxing a random magnetic configuration in the presence of strong damping ($\alpha = 0.5$). In the second, dynamic stage of the simulations, the static configuration was slightly perturbed by a harmonic dynamic external magnetic field $\mathbf{H}_\mathrm{dyn}(x, y, t) = H_x(x, y) \sin(2\pi f t)\, \hat{e}_x$ (i.e., $\mathbf{H} \perp \mathbf{H}_\mathrm{dyn}$) to induce continuous SW excitation. The frequency f of the field $\mathbf{H}_\mathrm{dyn}$ determines the frequency of the excited SWs. The spatial profile of this field, $H_x(x, y)$, and its correspondence to the SW dispersion determine the shape of the SW excitation and its direction of propagation [30]. The shape and amplitude of the dynamic field were designed to excite a Gaussian SW beam (see Appendix B for a detailed description of the SW beam generation procedure). The generated Gaussian SW beam was 500 nm wide in its waist and had a frequency $f = 100$ GHz. After sufficiently long continuous SW excitation, when the transmitted beam became clearly visible, data necessary for further analysis were acquired and saved. In the dynamic simulations we assumed a reduced finite value of the damping parameter, $\alpha = 0.0005$, [59] to ensure long-distance propagation of the SW beam.

The acquired simulation data were then processed in order to extract the reflectance R and transmittance T, and the GH shift Δ_t of the transmitted beam. Firstly, time-average SW intensity colormaps (SWICs) were drawn for all the simulation results, with the time-average SW intensity $I(x, y)$ calculated from the equation:

$$I(x, y) = \frac{f}{4} \int_0^{4/f} \left[m_x(x, y, t)\right]^2 \mathrm{d}t.$$

Then, the value of T was extracted as the ratio of the SW power flowing through a plane parallel to the interface and shifted from it by a distance x_0 and the SW power in reference simulation:

$$T = \left[\int_{y_0}^{y_1} I(x_0, y)\mathrm{d}y\right] / \left[\int_{y_0}^{y_1} I_\mathrm{ref}(x_0, y)\mathrm{d}y\right];$$

the integration limits y_0 and y_1 along the y-axis are indicated in Fig. 3(a) and (b) (bold gray lines), where they play the role of numerator and denominator integration limits, respectively. The reference simulation SWIC $I_\mathrm{ref}(x, y)$ was obtained from simulations performed for a uniform Py thin film without any perturbation in the interface area.

The reflectance R can be calculated in a similar way, with the intensity of SWs flowing through a surface located at the position $-x_0$, normalized with the reference simulation result at x_0:

$$R = \left[\int_{y_0}^{y_1} I(-x_0, y)\mathrm{d}y\right] / \left[\int_{y_0}^{y_1} I_\mathrm{ref}(x_0, y)\mathrm{d}y\right].$$

We used this approach to discard the influence of the finite damping in the MSs. The relation $R + T = 1$ is fulfilled with good accuracy by our simulation results.

A similar approach was used for extracting the GH shift from the simulation data [48]. By Gaussian fitting we extracted the positions of the centers of the intensity profiles $I(x, y_i)$ along many lines (over 100 of points i) perpendicular to the interface at $y = y_i$. Then, having the coordinates of the centers of the incident and transmitted beams, we calculated the coefficients of the straight lines corresponding to the beams (dashed black line in Fig. 3(a) and (b) for incident beam and dashed green line in Fig. 3(b) for transmitted beam). Finally, we calculated the GH shift Δ_t, i.e., the horizontal shift between the transmitted and reference beams. Because of the weak reflectance and an ambiguity in the choice of the reflection plane in the numerical extraction of the reference beam we do not estimate here the GH shift Δ_r of the reflected beam. It is noteworthy that the value of Δ_t is free of such ambiguity, since it does not depend on the choice of the interface position.

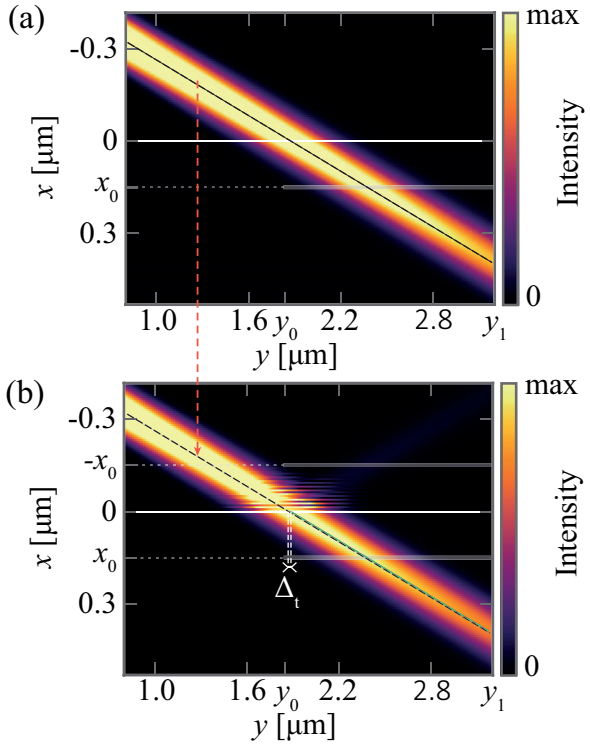

Figure 3. Sample results of the micromagnetic simulations for $\theta_i = 60°$, with intensity maps obtained from (a) the reference simulation of SW propagation in a homogeneous Py film, and (b) simulations of SWs transmitted through an interface with a strong magnetic anisotropy, $K_{12} = -4.5 \times 10^6$ erg/cm^3. The green dashed line in (b) is the ray of the refracted SW beam; the black dashed line is the ray of the reference beam, taken from (a). The horizontal white solid line represents the interface, and the horizontal gray solid lines the intervals used for calculating the intensities of the transmitted and reflected SW beams. The extracted value of the GH shift of the transmitted beam is $\Delta_t = 3.1$ nm.

III. RESULTS

A. Analytical model

Let us first analyze the results obtained from the analytical model for high-frequency SWs in a structure (schematically depicted in Fig. 1) composed of two semi-infinite Py films separated by an interface with a width much smaller than the wavelength of the SWs ($\delta \ll \lambda$). In the calculation of the effective material parameters in the interface region we assumed the same value of the interface width as in the micromagnetic simulations, $\delta = 2$ nm. The transmittance defined in Eqs. (11) and (9) is a symmetric function of K_{12}; obviously, for $K_{12} = 0$ (which corresponds to a homogeneous medium) reflection does not occur and $T = 1$. At a fixed angle of incidence the value of T decreases with increasing $|K_{12}|$ (see Fig. 4(a)); T decreases also with increasing angle of incidence (Fig. 4(c)). A similar behavior is observed in electromagnetic waves. However, in the case considered, at a fixed angle of incidence the transmission of SWs through an interface with an increased magnetic anisotropy increases with increasing SW frequency (Fig. 4(e)) [46].

In the case of identical materials with zero anisotropy ($K_1 = K_2 = 0$) the GH shifts for reflected and refracted SWs are equal, $\Delta_t = \Delta_r$. This results from identical expressions for the phase shifts φ_r and φ_t, see Eqs. (12) and (13). From those equations it also follows that the dependence of the GH shift on the magnetic anisotropy at the interface is an antisymmetric function of K_{12}, taking on positive or negative values for $K_{12} < 0$ and $K_{12} > 0$, respectively (see Fig. 4(b)). This is caused by the change from easy-axis to easy-plane magnetic anisotropy upon reversal of the sign of K_{12} [45].

The absolute value of the GH shift, $|\Delta_t|$, increases with increasing angle of incidence for $|K_{12}| \leq 6 \times 10^6$ erg/cm^3 (see Fig. 4(b) and (d)). As in other types of waves, the GH shift increases substantially with the angle of incidence, up to values comparable to the wavelength of the SWs (around 60 nm at 100 GHz). However, for absolute values $|K_{12}|$ of the magnetic anisotropy larger than those considered here $|\Delta_t|$ decreases to approach 0 in the limit $|K_{12}| \to \infty$. This dependence is similar to that observed in reflection by the edge of a ferromagnetic material with a surface anisotropy [45].

Another observation is a decrease in the GHS with increasing frequency, shown in Fig. 4(f). This implies small phase shifts in transmission of high-frequency SWs. In general, analysis of the plots in Fig. 4 leads to the conclusion that the GH shift increases with decreasing transmission. However, this only applies to a limited range of interface anisotropy constant values, i.e., until $|\Delta_t|$ reaches a maximum.

B. Simulations

The results of the analytical modeling were obtained for exchange SWs uniform along the z-axis, propagating in an infinitely thick material (Py). The micromagnetic simulations, however, take into account the dipolar interaction and the finite thickness of the sample; thus, in the MSs we investigate reflection and transmission of SWs in a thin-film system of finite thickness, consisting of two films connected by an edge interface with a width $\delta = 2$ nm (Fig. 3). The considered range of K_{12} values in the interface region is $|K_{12}| \leq 4.5 \times 10^6$ erg/cm^3, a physically realistic magnetic anisotropy [47]. Note that in pure Py the volume anisotropy is usually negligible.

Figure 5 shows T (left column) and Δ_t (right column) plotted vs. K_{12} for three angles of incidence: 45°, 60° and 70°. The simulation results are represented by red dashed lines and labeled with a subscript s. These results are qualitatively consistent with those obtained from the analytical model (green dashed lines and subscript a in Fig. 5). However, the transmittance values are higher and the GH shifts smaller than the respective analytical

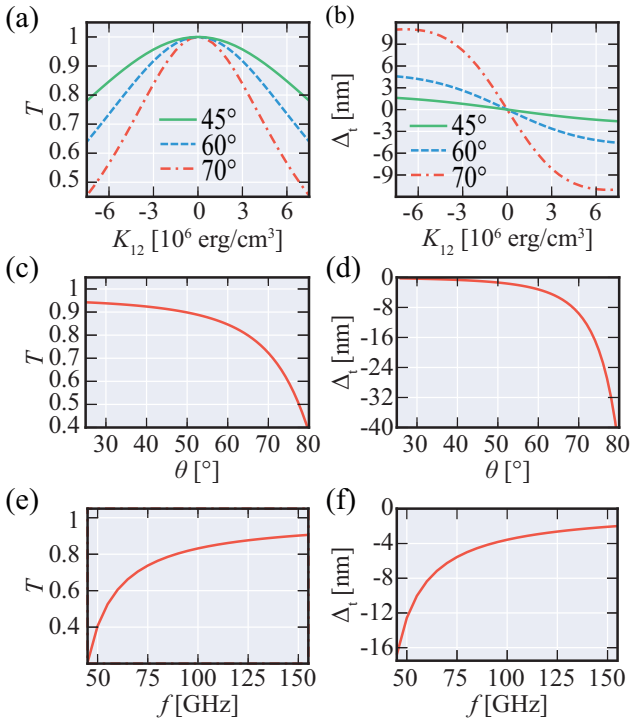

Figure 4. (a) Transmittance and (b) GH shift vs. magnetic anisotropy at the interface between two semi-infinite materials (Py). Green solid, blue dashed and red dash-dotted lines correspond to different angles of incidence θ_i: 45°, 60° and 70°, respectively. (c) Transmittance and (d) GH shift vs. angle of incidence for $K_{12} = 4.5$ erg/cm^3. Plots (a)-(d) were obtained for SWs of frequency $f = 100$ GHz. (e) Transmittance and (f) GH shift vs. frequency for $K_{12} = 4.5$ erg/cm^3 and $\theta_i = 60°$. The results presented in this Figure were obtained for $H_0 = 15$ kOe.

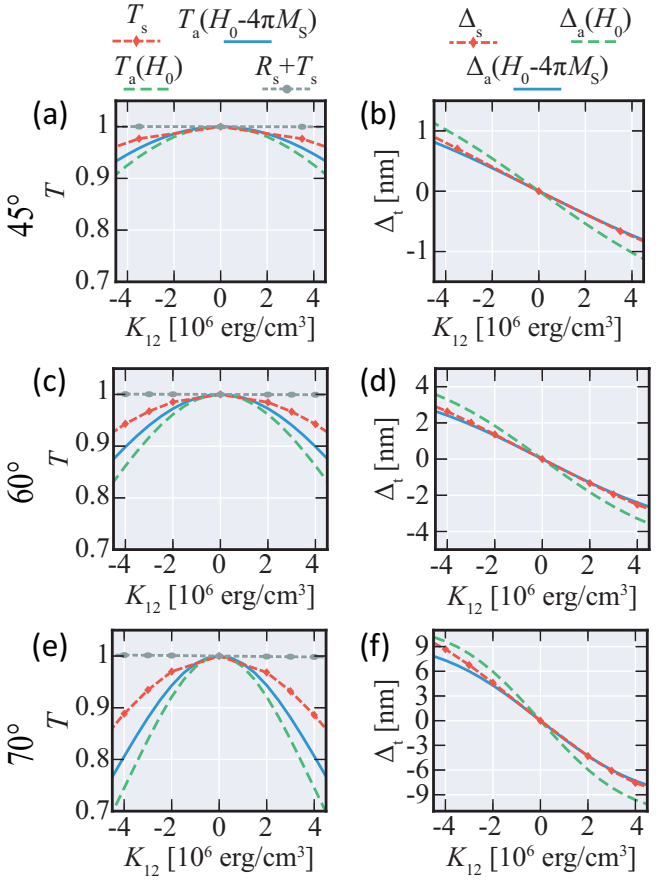

Figure 5. Analytical results and simulation data. The MS results (red dashed lines with diamonds) were obtained for a Py thin film divided by an interface with anisotropy K_{12}. In the analytical model we considered two semi-infinite materials (Py) separated by an interface plane with anisotropy K_{12}, with internal magnetic field H_0 (green dashed lines), later artificially reduced to $H_0 - 4\pi M_S$ (blue solid line). (a), (c), (e) Transmittance versus K_{12} for angles of incidence 45°, 60° and 70°, respectively. Plotted as a dashed gray line with circles, the sum of the MS values of transmittance and reflectance is in very good approximation equal to 1. (b), (d), (f) Goos-Hänchen shift Δ_t vs. K_{12} for angles of incidence 45°, 60° and 70°, respectively.

results.

We suppose this is due to the finite thickness of the Py film and the dipolar interaction in the MSs. In the perpendicular configuration of the magnetization with respect to the film plane the dipolar interaction creates a strong static demagnetizing field, which reduces the internal magnetic field by $4\pi M_S$. Indeed, the substitution of a reduced value of the external magnetic field $H_0' = H_0 - 4\pi M_S$ for H_0 in the analytical formulas (9) and (14) for T and Δ_t provides a far better match between the analytical results and the simulation data (see Fig. 5, where the updated analytical results are plotted as solid blue lines).

However, the MS values of transmittance are still higher than those obtained from the analytical model. The difference increases with the angle of incidence and with $|K_{12}|$. We think this increase in transmission may result from the dynamic magnetostatic interaction, which is neglected in the model.

The GH shift obtained from Eq. (14) with the reduced magnetic field is in very good agreement with the MS results. Still, there are some discrepancies for large angles of incidence and negative values of K_{12} (see Fig. 5(f) for $\theta_i = 70°$ and $K_{12} < 0$). Below we address this asymmetry observed in the $\Delta_t(K_{12})$ function.

Let us analyze how the transmission of SWs changes with decreasing SW frequency in this context. Figure 6 shows the results of MSs with the same structure as above, for $\theta_i = 60°$ and five different frequencies: 100 GHz, 75 GHz, 50 GHz, 40 GHz and 30 GHz. As predicted analytically (Fig. 5), the transmittance decreases and the absolute value of the GH shift increases with decreasing SW frequency. However, as the SW frequency decreases, the $\Delta_t(K_{12})$ function becomes increasingly asymmetric: for negative values of K_{12} the absolute value of the GH shift is larger than for positive

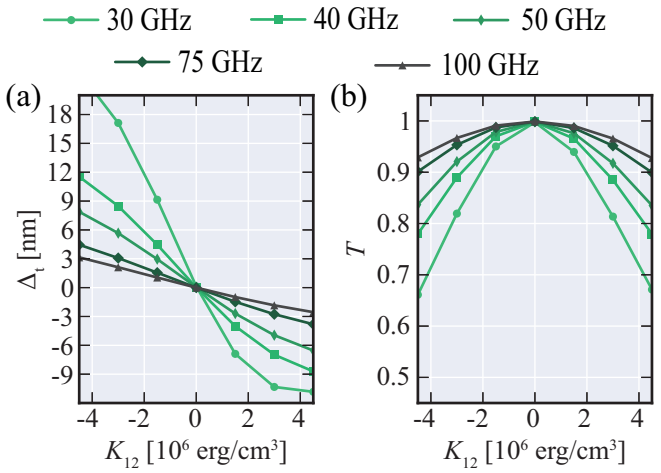

Figure 6. Results of MSs for a Py film divided by an interface with anisotropy K_{12}: (a) Δ_t and (b) T versus K_{12} for five SW frequencies, 30 GHz, 40 GHz, 50 GHz, 75 GHz and 100 GHz. The angle of incidence is 60°.

anisotropy values (see, e.g., the dependence for 30 GHz, represented by a line with full dots in Fig. 6(a), or the plot in Fig. 5(f)).

The analytical model was developed for purely exchange SWs, and further extended by including the static demagnetizing field. This approximation is well suited to high-frequency SWs. However, with decreasing SW frequency the role of the dynamic dipolar interaction increases, and larger discrepancies between analytical results and simulation data can be expected.

We attribute the observed differences in transmittance to the dynamic dipolar interaction (at $K_{12} = -4.5 \times 10^6$ the discrepancy between the analytical predictions and the MS results grows from 0.05 for 100 GHz to 0.1 for 50 GHz). However, the influence of the dipolar interaction on SW transmission has not been fully elucidated to date; this requires the development of a new model, which goes beyond the scope of this paper.

Nevertheless, the dipolar interaction does not provide explanation of the asymmetry, also increasing with decreasing SW frequency in the MSs, in the K_{12} dependence of the GH shift. We suppose it is due to different SW polarizations at the interface for positive and negative K_{12} (easy axis and easy plane, respectively). In the case of $K_{12} < 0$ an increase of the m_y component with respect to m_x can be expected (and is confirmed by MSs), resulting in a larger GH shift along the y-axis. Indeed, whereas for $K_{12} > 0$ the GH shift obtained in the simulations is in good agreement with the analytical results (with circular precession of the magnetization assumed), as shown in Fig. 5(f), for $K_{12} < 0$ the MS values of Δ_t are larger and the difference increases with decreasing K_{12}.

IV. SUMMARY

We have studied theoretically the reflection and transmission of obliquely incident SWs by a thin interface between two extended ferromagnetic media and between two semi-infinite films connected by an edge. The interface area has a different uniaxial anisotropy with respect to the extended areas. We have derived analytical formulas describing the reflectance and transmittance of exchange SWs, as well as the phase shifts and lateral GH shifts for refracted and reflected SWs. Moreover, using micromagnetic simulations we have demonstrated that these results of analytical modeling also describe qualitatively SWs in the thin-film geometry. It is noteworthy that, in spite of a number of assumptions in the analytical approach (negligible dipolar interaction, infinite extent of the ferromagnetic materials, and circular precession of SWs), the results obtained by the two techniques are in very good agreement for high-frequency SWs.

In the numerical study we have focused on the transmission of SWs and the related GH shift. The GH shift of transmitted SWs proves to increase with increasing anisotropy in the interface region and with decreasing SW frequency. We point out the increased role of the dynamic dipolar interaction in SW transmission, and the influence of the elliptical polarization of the SW beam at the interface on the GH shift at lower frequencies. The influence of these two factors on the GH shift of transmitted SWs needs to be elucidated in detail, which requires further investigation and the development of a new analytical model.

The demonstrated lateral GH shift of SWs refracted by an interface with a width much smaller than the wavelength of the considered waves points to the possibility of steering SWs in thin films at sub-wavelength distances. Although the lateral shift found in a Py thin film divided in two parts by a narrow (2 nm wide) interface with increased magnetic anisotropy is not significant, we have shown possible ways to increase it. Further investigation can lead to the development of more methods of phase modulation at sub-wavelength distances. This sets a promising direction in the study of magnonic metasurfaces, a novel field in magnonics, next to the graded index magnonics [54].

In the present paper we have also proposed an efficient method for the excitation of SW beams, which should be of use in further numerical investigations.

APPENDIX A

The formula for the lateral GH shift of SWs reflected by an interface between two ferromagnetic materials reads:

$$\Delta_{\mathrm{r}} = -\frac{\partial \varphi_{\mathrm{r}}}{\partial k_{\mathrm{r},y}} = \\ = -\frac{\frac{\alpha_1 k_{\mathrm{r},y}}{\sqrt{k_1^2 - k_{\mathrm{r},y}^2}}\left(D\alpha_2^2\left(k_{\mathrm{t}}^2 - k_{\mathrm{r},y}^2\right) - C\left(A_{12}^2 - CD\right)\right) + \frac{\alpha_2 k_{\mathrm{r},y}}{\sqrt{k_{\mathrm{t}}^2 - k_{\mathrm{r},y}^2}}\left(C\alpha_1^2\left(k_{\mathrm{r}}^2 - k_{\mathrm{r},y}^2\right) - D\left(A_{12}^2 - CD\right)\right)}{\left(A_{12}^2 - CD + \alpha_1\alpha_2\sqrt{k_{\mathrm{r}}^2 - k_{\mathrm{r},y}^2}\sqrt{k_{\mathrm{t}}^2 - k_{\mathrm{r},y}^2}\right)^2 + \left(C\alpha_1\sqrt{k_{\mathrm{r}}^2 - k_{\mathrm{r},y}^2} + D\alpha_2\sqrt{k_{\mathrm{t}}^2 - k_{\mathrm{r},y}^2}\right)^2} \\ -\frac{\frac{\alpha_1 k_{\mathrm{r},y}^2}{\sqrt{k_{\mathrm{r}}^2 - k_{\mathrm{r},y}^2}}\left(D\alpha_2^2\left(k_{\mathrm{t}}^2 - k_{\mathrm{r},y}^2\right) - C\left(A_{12}^2 - CD\right)\right) - \frac{\alpha_2 k_{\mathrm{r},y}}{\sqrt{k_{\mathrm{t}}^2 - k_{\mathrm{r},y}^2}}\left(C\alpha_1^2\left(k_{\mathrm{r}}^2 - k_{\mathrm{r}\|}^2\right) - D\left(A_{12}^2 - CD\right)\right)}{\left(A_{12}^2 - CD - \alpha_1\alpha_2\sqrt{k_{\mathrm{r}}^2 - k_{\mathrm{r},y}^2}\sqrt{k_{\mathrm{t}}^2 - k_{\mathrm{r},y}^2}\right)^2 + \left(C\alpha_1\sqrt{k_{\mathrm{r}}^2 - k_{\mathrm{r},y}^2} - D\alpha_2\sqrt{k_{\mathrm{t}}^2 - k_{\mathrm{r},y}^2}\right)^2}. \tag{15}$$

For SWs transmitted through the interface the GH shift is expressed by the equation:

$$\Delta_{\mathrm{t}} = -\frac{\partial \varphi_{\mathrm{t}}}{\partial k_{\mathrm{t},y}} = \\ = -\frac{\frac{\alpha_1 k_{\mathrm{r},y}}{\sqrt{k_{\mathrm{r}}^2 - k_{\mathrm{r},y}^2}}\left(D\alpha_2^2\left(k_{\mathrm{t}}^2 - k_{\mathrm{r},y}^2\right) - C\left(A_{12}^2 - CD\right)\right) + \frac{\alpha_2 k_{\mathrm{r},y}}{\sqrt{k_{\mathrm{t}}^2 - k_{\mathrm{r},y}^2}}\left(C\alpha_1^2\left(k_{\mathrm{r}}^2 - k_{\mathrm{r},y}^2\right) - D\left(A_{12}^2 - CD\right)\right)}{\left(A_{12}^2 - CD + \alpha_1\alpha_2\sqrt{k_{\mathrm{r}}^2 - k_{\mathrm{r},y}^2}\sqrt{k_{\mathrm{t}}^2 - k_{\mathrm{r},y}^2}\right)^2 + \left(C\alpha_1\sqrt{k_{\mathrm{r}}^2 - k_{\mathrm{r},y}^2} + D\alpha_2\sqrt{k_{\mathrm{t}}^2 - k_{\mathrm{r},y}^2}\right)^2}. \tag{16}$$

APPENDIX B: SPIN-WAVE BEAM EXCITATION METHOD FOR MICROMAGNETIC SIMULATIONS

In our previous papers [45, 48] we used a simple method for the excitation of a SW beam with a wavevector parallel to the x-axis, based on the application of an external microwave magnetic field in the form $H_{\mathrm{dyn}}(x,y) = h\Theta_{\mathrm{H}}(x + w/2)\Theta_{\mathrm{H}}(-x + w/2)G(y)$, where Θ_{H} is the Heaviside step function, $G(y)$ is the Gaussian distribution function $G(x) = \exp\left[2x^2/\left(L\sigma\right)^2\right]$, w denotes length, L is the width of the excitation area, and $\sigma \leq 0.2$. This method is very simple to implement in MSs and provides good quality beams in most cases. However, it is far from experimental realization and involves the excitation of some additional, undesirable waves due to the finite discretization used in the finite difference method. Usually this disadvantage can be neglected, but in our study, which required very high accuracy for the determination of the GH shifts, the additional waves represented a substantial interference. Therefore we have developed an advanced SW beam excitation method, in which numerical artifacts due to discretization of the applied magnetic field are almost entirely eliminated. Moreover, the profiles of the applied field are more realistic [30] than those used previously [45, 48].

Let us assume a dynamic field in the form:

$$H_x(x,y,t) = A(x,y)B(y)\sin\left(2\pi f t\right), \tag{17}$$

where the function $B(y)$ describes the envelope of the magnetic field amplitude along the y-axis. Usually, especially in the case of SW excitation in waveguides or in homogeneous structures, we can assume $B(y) = 1$. However, sometimes, particularly for oblique SW beam excitation in planar structures, other envelopes should be used, which we will present later.

The function $A(x,y)$ approximates the profile of the field generated by a coplanar waveguide antenna [30]:

$$A(x,y) = C \quad \left[\frac{1}{(x+x_1(y))^2+1} - \frac{1}{(x+x_0(y))^2+1} - \frac{1}{(x-x_0(y))^2+1} + \frac{1}{(x-x_1(y))^2+1}\right], \tag{18}$$

where C is a constant, the value of which determines the maximal value of H_x.

The functions $x_0(y)$ and $x_1(y)$ describe the geometry of the generated field and determine the efficiency of SW excitation. According to an analysis presented in Ref. [30], for such a profile the maximally efficient resonant excitation of SWs with a wavelength λ is achieved when $x_0(0)$ and $x_1(0)$ fulfill the equation:

$$\frac{2}{\lambda} = \frac{1}{x_0(0) + x_1(0)}, \tag{19}$$

where λ is a function of frequency, $\lambda(f) = 2\pi/k(f)$, via the inverse dispersion relation $k(f)$.

In the case of exchange-dominated SWs Eq. (4) can be used; the general dispersion relation is presented in Ref. [53].

On the other hand, with the geometrical parameters $x_0(y_{\mathrm{nE}})$ and $x_1(y_{\mathrm{nE}})$ fulfilling the equation:

$$\frac{1}{\lambda} = \frac{1}{x_0(y_{\mathrm{nE}}) + x_1(y_{\mathrm{nE}})}, \tag{20}$$

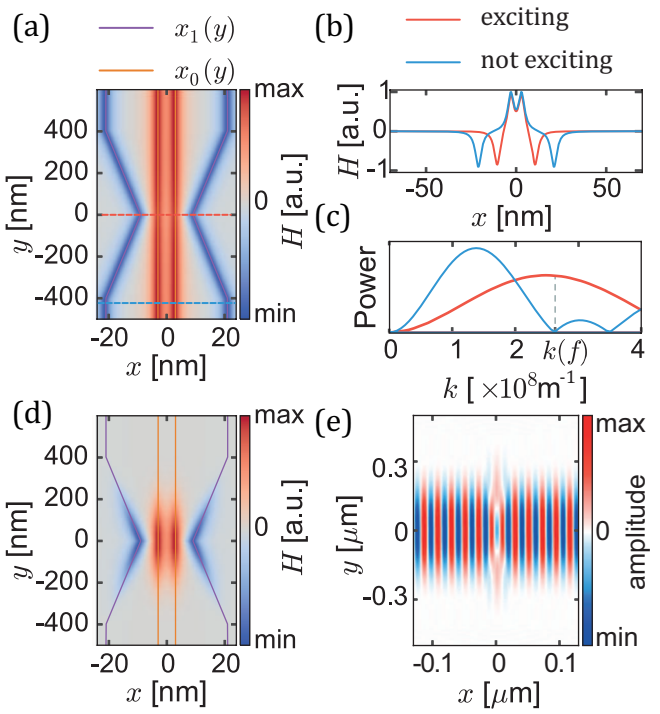

Figure 7. (a) Profile of dynamic magnetic field $H_{\rm dyn}$ for $B(y) = 1$. (b) Magnetic field profiles along the x-axis: $H_1 = H_x(y = 0)$ (red line) and $H_2 = H_x(y = L/2)$ (blue line). (c) Fourier transforms of the magnetic field profiles presented in (b): $\widetilde{H}_1 = \mathcal{F}\{H_1\}$ (red) and $\widetilde{H}_2 = \mathcal{F}\{H_2\}$ (blue). Note that $\widetilde{H}_1$ has a maximum for $k = k(f)$ corresponding to a zero of $\widetilde{H}_2$. (d) Profile of dynamic magnetic field $H_{\rm dyn}$ for $B(y) = G(y)$. (e) Sample SW beam excited using the dynamic magnetic field profile (d).

the excitation of SWs will be inefficient. The solution of this set of equations leads to:

$$2x_0(0) + 2x_1(0) = x_0(y_{\rm nE}) + x_1(y_{\rm nE}). \qquad (21)$$

For simplicity, let us assume a constant value of $x_0(y) \equiv x_0$. Thus:

$$x_1(y_{\rm nE}) = x_0 + 2x_1(0). \qquad (22)$$

We assume $x_1(y)$ is a continuous linear function:

$$x_1(y) = x_1(0) + \frac{2}{L}\left[x_0 + x_1(0)\right] y, \qquad (23)$$

where $L/2 = y_{\rm nE}$ is the length over which the value of $x_1(y)$ changes from $x_1(0)$ (corresponding to resonant SW excitation) to $x_1(y_{\rm nE})$ (corresponding to inefficient SW excitation). Note that L can be regarded as the length of the antenna; for $y > L/2$ SWs will not be excited.

This approach only applies to the case $L \gg \lambda$. Moreover, the substitution of $G(y)$ for $B(y)$ is recommended for further improvement of the quality of the simulated beam. Alternatively, sech^2 can be used instead of the Gaussian function as an additional envelope of the dynamic magnetic field.

In the MSs presented in this paper 500 nm wide SW beams were excited with the following parameter values: $L = 1200$ nm, $\sigma^2 = 0.1$ and $C = 0.02H_0$.

ACKNOWLEDGMENTS

This project has received funding from the European Union's Horizon 2020 research and innovation programme under Marie Skłodowska-Curie grant agreement no. 644348, and from the Polish National Science Centre, project UMO-2012/07/E/ST3/00538. P.G. also acknowledges support from Adam Mickiewicz University Foundation. The numerical calculations were performed at Poznan Supercomputing and Networking Center (grant no. 209).

[1] G. E. Moore, Cramming more components onto integrated circuits, Electronics **38**, 8 (1965).
[2] M. Mitchell Waldrop, The chips are down for Moore's law, Nature **530**, 144 (2016).
[3] S. Lloyd, Ultimate physical limits to computation, Nature **406**, 1047 (2000).
[4] K. Bernstein, R. C. Cavin, W. Porod, A. Seabaugh, and J. Welser, Device and architecture outlook for beyond CMOS switches, Proceedings of the IEEE **98**, 2169 (2010).
[5] D. Nikonov and I. A. Young, Overview of beyond-CMOS devices and a uniform methodology for their benchmarking, Proceedings of the IEEE **101**, 2498 (2013).
[6] M. Krawczyk and D. Grundler, Review and prospects of magnonic crystals and devices with reprogrammable band structure, J. Phys.: Condens. Matter **26**, 123202 (2014).
[7] A. V. Chumak, A. A. Serga and B. Hillebrands, Magnon transistor for all-magnon data processing, Nat. Commun. **5**, 4700 (2014).
[8] Editorial: The next wave, Nat. Phys. **11**, 437 (2015).
[9] V. V. Kruglyak, S. O. Demokritov and D. Grundler, Magnonics, J. Phys. D: Appl. Phys. **43**, 264001 (2010).
[10] S. O. Demokritov and A. N. Slavin (eds.) Magnonics from fundamentals to applications (Berlin: Springer, 2013).
[11] A. V. Chumak, V. I. Vasyuchka, A. A. Serga and B. Hillebrands, Magnon Spintronics, Nature Phys. 11, 453 (2015).
[12] A. Kozhevnikov, F. Gertz, G. Dudko, Y. Filimonov, and A. Khitun, Pattern recognition with magnonic holographic memory device, Appl. Phys. Lett. **106**, 142409 (2015).

[13] G. Csaba, A. Papp, and W. Porod, Spin-wave based realization of optical computing primitives, J. Appl. Phys. **115**, 17C741 (2014).

[14] F. Gertz, A. Kozhevnikov, Y. Filimonov, and A. Khitun, Magnonic holographic read-only memory, IEEE Magn. Lett. **7**, 3200204 (2016).

[15] N. Locatelli, V. Cros, and J. Grollier, Spin-torque building blocks, Nat. Mater. **13**, 11 (2014).

[16] S. Macke and D. Goll, Transmission and reflection of spin waves in the presence of Neel walls, J. Phys.: Conf. Ser. **200**, 042015 (2010).

[17] N. Yu, and F. Capasso, Flat optics with designer metasurfaces, Nat. Mater. **13**, 139 (2014).

[18] A. V. Chumak, A. A. Serga, S. Wolff, B. Hillebrands, and M. P. Kostylev, Scattering of surface and volume spin waves in a magnonic crystal, Appl. Phys. Lett. **94**, 172511 (2009).

[19] S.-K. Kim, S. Choi, K.-S. Lee, D.-S. Han, D.-E. Jung, and Y.-S. Choi, Negative refraction of dipole-exchange spin waves through a magnetic twin interface in restricted geometry, Appl. Phys. Lett. **92**, 212501 (2008).

[20] J. W. Kłos, P. Gruszecki, A. E. Serebryannikov, and M. Krawczyk, All-angle collimation for spin saves, IEEE Magn. Let. **6**, 3500804 (2015).

[21] J. Stigloher, M. Decker, H. S. Körner, K. Tanabe, T. Moriyama, T. Taniguchi, H. Hata, M. Madami, G. Gubbiotti, K. Kobayashi, T. Ono, and C. H. Back, Snell's law for spin waves, Phys. Rev. Lett. **117**, 037204 (2016).

[22] G. A. Vugal'Ter, and A. G. Korovin, Propagation of surface-magnetostatic-wave beams in a ferrite film, Radiofizika **31**, 1126 (1988).

[23] R. E. Floyd and J. C. Sethares, MSFVW beam steering and spreading over large path lengths, J. Appl. Phys. **55**, 2515 (1984).

[24] T. Schneider, A. V. Chumak, C. W. Sandweg, S. Trudel, S. Wolff, M. P. Kostylev, V. S. Tiberkevich, A. N. Slavin, and B. Hillebrands, Nondiffractive subwavelength wave beams in a medium with externally controlled anisotropy, Phys. Rev. Lett. **104**, 197203 (2010).

[25] R. Gieniusz, H. Ulrichs, V. D. Bessonov, U. Guzowska, A. I. Stognii, and A. Maziewski, Single antidot as a passive way to create caustic spin-wave beams in yttrium iron garnet films, Appl. Phys. Lett. **102**, 102409 (2013).

[26] M. P. Kostylev, A. A. Serga, and B. Hillebrands, Radiation of caustic beams from a collapsing bullet, Phys. Rev. Lett. **106**, 134101 (2011).

[27] J. W. Boyle, S. A. Nikitov, A. D. Boardman, J. G. Booth, and K. Booth, Nonlinear self-channeling and beam shaping of magnetostatic waves in ferromagnetic films, Phys. Rev. B **53**, 12173 (1996).

[28] M. Bauer, C. Mathieu, S. O. Demokritov, B. Hillebrands, P. A. Kolodin, S. Sure, H. Dötsch, V. Grimalsky, Yu. Rapoport, and A. N. Slavin, Direct observation of two-dimensional self-focusing of spin waves in magnetic films, Phys. Rev. B **56**, R8483 (1997).

[29] A. Houshang, E. Iacocca, P. Dürrenfeld, S. R. Sani, J. Akerman & R. K. Dumas, Spin-wave-beam driven synchronization of nanocontact spin-torque oscillators, Nature Nanotechnology **2015**, 280 (2015).

[30] P. Gruszecki, M. Kasprzak, A. E. Serebryannikov, W. Smigaj, and M. Krawczyk, Microwave excitation of spin wave beams in thin ferromagnetic films, Sci. Rep. **6**, 22367 (2016).

[31] H. Hänchen, and F. Goos, Ein neuer fundamentaler versuch zur totalreflection, Ann. Phys. (Leipzig) **436**, 333 (1947).

[32] N. F. Declercq, and E. Lamkanfi, Study by means of liquid side acoustic barrier of the influence of leaky Rayleigh waves on bounded beam reflection, Appl. Phys. Lett. **93**, 054103 (2008).

[33] X. Chen, X.-J. Lu, Y. Ban, and C.-F. Li, Electronic analogy of the Goos-Hänchen effect: a review, J. Opt. **15**, 033001 (2013).

[34] V.-O. de Haan, J. Plomp, T. M. Rekveldt, W. H. Kraan, A. A. van Well, R. M. Dalgliesh, and S. Langridge, Observation of the Goos-Hänchen shift with neutrons, Phys. Rev. Lett. **104**, 010401 (2010).

[35] K. Yasumoto, and Y. Oishi, A new evaluation of the Goos-Hänchen shift and associated time delay, J. Appl. Phys. **54**, 2170 (1983).

[36] Yu. S. Dadoenkova, N. N. Dadoenkova, I. L. Lyubchanskii, M. L. Sokolovskyy, and J. W. Klos, Huge Goos-Hänchen effect for spin waves: A promising way to study magnetic properties at interfaces, Appl. Phys. Lett. **101**, 042404 (2012).

[37] V.V. Kruglyak, O.Yu. Gorobets, Yu.I. Gorobets and A.N. Kuchko, Magnetization boundary conditions at a ferromagnetic interface of finite thickness, J. Phys.: Condens. Matter **26**, 406001 (2014).

[38] A.M. Kosevich, B.A. Ivanov, and A.S. Kovalev, Nonlinear magnetization waves. Dynamic and topological solitons (Naukova Dumka, Kiev 1983).

[39] K. Artmann, Berechnung der Seitenversetzung des totalreflektierten Strahles, Ann. Phys. (Leipzig) **2**, 87 (1948).

[40] S.A. Reshetnyak, The approximation of geometrical optics for bulk spin waves in spatially inhomogeneous ferromagnetic insulators with an exchange defect, Low Temp. Phys. **30**, 295 (2004).

[41] O.Yu. Gorobets, Yu.I. Gorobets, T.Yu. Rospotniuk, V.P. Rospotniuk Propagation of spin waves through anisotropic interface between two ferromagnets in an external magnetic field. Research Bulletin of National Technical University of Ukraine "Kyiv Polytechnic Institute **4**, 119 (2014).

[42] S.A. Reshetnyak, Refraction of surface spin waves in a spatially nonuniform ferrodielectrics with two-axial magnetic anisotropy, Sol. Stat. Phys. **46**, 1031 (2004).

[43] A. Puri and J. L. Birman Goos-Hänchen beam shift at total internal reflection with application to spatially dispersive media, J. Opt. Soc. Am. A **3**, 543 (1986).

[44] A. Vansteenkiste, J. Leliaert, M. Dvornik, M. Helsen, F. Garcia-Sanchez and B. Van Waeyenberge, The design and verification of MuMax3, AIP Advances **4**, 107133 (2014).

[45] P. Gruszecki, J. Romero-Vivas, Yu. S. Dadoenkova, N. N. Dadoenkova, I. L. Lyubchanskii and M. Krawczyk, Goos-Hänchen effect and bending of spin wave beams in thin magnetic films, Appl. Phys. Lett. **105**, 242406 (2014).

[46] Yu. I. Gorobets and S. A. Reshetnyak, Reflection and refraction of spin waves in uniaxial magnets in the geometrical-optics approximation, Techn. Phys. **43**, 2 (1998).

[47] C. A. F. Vaz, J. A. C. Bland, and G. Lauhoff, Magnetism in ultrathin film structures, Rep. Prog. Phys. **71**, 056501 (2008).

[48] P. Gruszecki, Yu. S. Dadoenkova, N. N. Dadoenkova, I. L. Lyubchanskii, J. Romero-Vivas, K. Y. Guslienko, and M. Krawczyk, Influence of magnetic surface anisotropy

on spin wave reflection from the edge of ferromagnetic film, Phys. Rev. B **92**, 054427 (2015).

[49] G. Venkat, D. Kumar, M. Franchin, O. Dmytriiev, M. Mruczkiewicz, H. Fangohr, A. Barman, M. Krawczyk, and A. Prabhakar, Proposal for a standard micromagnetic problem: Spin wave dispersion in a magnonic waveguide, IEEE Trans. Magn. **49**, 524 (2013).

[50] W. Kim, S.-W. Lee and K.-J. Lee, Micromagnetic modelling on magnetization dynamics in nanopillars driven by spin-transfer torque, J. Phys. D: Appl. Phys. **44**, 384001 (2011).

[51] R. Hertel, W. Wulfhekel, and J. Kirschner, Domain-wall induced phase shifts in spin waves, Phys. Rev. Lett. **93**, 257202 (2004).

[52] K. M. Lebecki, M. J. Donahue, and M. W. Gutowski, Periodic boundary conditions for demagnetization interactions in micromagnetic simulations, J. Phys. D, Appl. Phys. **41**, 175005 (2008).

[53] B. A. Kalinikos and A. N. Slavin, Theory of dipole-exchange spin wave spectrum for ferromagnetic films with mixed exchange boundary conditions, J. Phys. C: Solid State Phys. **19**, 7013 (1986).

[54] C. S. Davies, A. Francis, A. V. Sadovnikov, S. V. Chertopalov, M. T. Bryan, S. V. Grishin, D. A. Allwood, Y. P. Sharaevskii, S. A. Nikitov, and V. V. Kruglyak, Towards graded-index magnonics: Steering spin waves in magnonic networks, Phys. Rev. B **92**, 020408(R) (2015).

[55] M. A. W. Schoen, D. Thonig, M. L. Schneider, T. J. Silva, H. T. Nembach, O. Eriksson, O. Karis, and J. M. Shaw, Ultra-low magnetic damping of a metallic ferromagnet, Nature Physics 12, 839–842 (2016).

[56] C. Liu, C. K. A. Mewes, M. Chshiev, T. Mewes, and W. H. Butler, Origin of low Gilbert damping in half metals, Appl. Phys. Lett. 95, 022509 (2009).

[57] Hauser et al., Yttrium iron garnet thin films with very low damping obtained by recrystallization of amorphous material, Scientific Reports 6 20827 (2016).

[58] Since $\delta \ll \lambda$ (where λ is the wavelength of the SWs), the assumption of integration limits -0 and $+0$ maintains finite effective material parameters describing the interface [38].

[59] A small value of damping was used in the MSs to ensure sufficiently large amplitudes of reflected and transmitted SWs. However, additional simulations performed for stronger damping show that it does not have a significant influence on the results obtained. The same physics can be found in other materials, including $Co_{25}Fe_{75}$[55], Heusler alloys [56] or YIG [57], where damping can be even smaller than that assumed in this paper.